22nd Australasian Fluid Mechanics Conference AFMC2020
Brisbane, Australia, 7–10 December 2020
https://doi.org/10.14264/3538538

Wedge shaped protrusions in duct flows for heat transfer enhancement

S. Murali[1] **and G. J. Sheard**[1]

[1] Department of Mechanical & Aerospace Engineering
Monash University, VIC 3800, Australia

Abstract

Understanding the underlying fluid dynamics is essential for the design of ducts and control of flow therein such that better heat transfer efficiency could be achieved. The numerical results of flow through a duct with repeated wedge-shaped protrusions heated from below with the aim to investigate the effect of such protrusions for heat transfer enhancement are presented. Different flow regimes for a two-dimensional flow are identified and the heat transfer enhancement achieved by varying two different geometric parameters of the wedge (blockage and distance between the wedges - pitch) are explained. Three-dimensional linear stability limits and the underlying modes which destabilises the flow are unveiled and the effect of three-dimensionality on the heat transfer behaviour are elucidated. Further, sensitive regions in the flow wherein any modification will be beneficial to amplify instabilities and control these flows for better heat transfer enhancement are discussed.

Keywords
Heat transfer enhancement; linear stability; sensitivity

Introduction

This study draws motivation from the cooling blanket ducts in magnetic confinement nuclear fusion reactors where there is a need to enhance the heat transfer efficiency from the fusion reactor to the cooling blanket fluid [16]. Bluff bodies [5, 3], point electrodes [5] and variable surface conductivity [6] have been used in previous studies for vortex promotion. Use of surface geometric modification has not been explored as means to enhance heat transfer in magnetohydrodynamic duct flows, in contrast to the hydrodynamic case. Most of these studies have had a focus on high Reynolds number (*Re*) turbulent flows [8, 2]. Flow in a duct having a wedge shaped surface geometry have been considered, as this gometry was found to outperform rectangular and other geometries in terms of heat transfer efficiency in high *Re* flows [2]. In the cooling blankets of fusion reactors, the flow conditions are generally in the steady or transitional regimes [16]. So, our focus is on these flow regimes. Further, understanding the underlying dynamics leading to transition can help to understand the system better which in turn will be beneficial for design and control of flows to enhance the performance of the system.

The aim of this study is to understand the onset of transition in duct flows with repeated wedge shaped protrusions and its effectiveness to promote heat transfer efficiency. Duct flow here is a pressure driven channel flow with infinite spanwise length. The enhancement achieved for a range of geometric parameters, covering the steady and unsteady regimes are presented. Furthermore, possible regions in the flow where it could be favourable to have a control mechanism for increasing instabilities and a possibility for heat transfer enhancement are presented.

Problem Setup and Methodology

The problem under consideration is shown in figure 1. A periodic streamwise flow domain with a constant temperature hot bottom wall and a constant-temperature cold top wall is considered. Two dimensionless geometric parameters are identified: blockage (β) - ratio of wedge height (h_w) to duct height ($2H$), and pitch (γ) - ratio of the distance between wedges l_p to half-duct height (H). The parameters considered in the study are: *Re* in the range 50–1300, $\beta = 0.125,0.25,0.5,0.65$, $\gamma = 1,2,3,4,5,8$ and Prandtl number $Pr = 6.14$ representative of water.

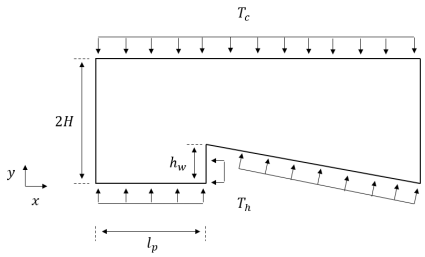

Figure 1. Flow geometry with periodic boundaries in the streamwise direction (x). Flow is left to right.

The dimensionless continuity, momentum and energy equations used for the computations are:

$$\boldsymbol{\nabla}\cdot\boldsymbol{u} = 0, \tag{1}$$

$$\frac{\partial \boldsymbol{u}}{\partial t} + (\boldsymbol{u}\cdot\boldsymbol{\nabla})\boldsymbol{u} = -\boldsymbol{\nabla}p + \frac{1}{Re}\boldsymbol{\nabla}^2\boldsymbol{u}, \tag{2}$$

$$\frac{\partial T}{\partial t} + (\boldsymbol{u}\cdot\boldsymbol{\nabla})T = \frac{1}{Pe}\boldsymbol{\nabla}^2 T. \tag{3}$$

where $\boldsymbol{u}$, p and T are the velocity, pressure and temperature fields respectively. Reynolds number and Peclet number are defined as $Re = U_0 H/\nu$ and $Pe = RePr$ respectively. Prandtl number $Pr = \nu/\kappa$, where ν and κ are the kinematic viscosity and thermal diffusivity respectively. Lengths are scaled by half-duct height H, velocity by the mean duct velocity U_0, time t by H/U_0, pressure by ρU_0^2 (where ρ is the fluid density) and temperature T by the difference in temperature between the hot and cold walls $\Delta T = T_h - T_c$.

Enhancement ratio (ER) is defined as the ratio of the heat transfer rate in the duct with wedges over that of a plane duct without the wedge to the pressure drop in the duct with wedges to that of a plane duct without the wedge, given by $ER = (Nu/Nu_0)/(f/f_0)$, where Nu, f, Nu_0 and f_0 are the Nusselt number and friction factor for the present flow domain and that of a plane duct without the wedge, respectively. Nusselt number is defined as the ratio of the transverse convective to the conductive heat transfer to the fluid, given by $Nu = hH/k$, where h is the convective heat transfer coefficient and k is the thermal conductivity of the fluid.

Linear stability analysis is used to study the stability of the 2D base flow by perturbing the base flow variables, $\boldsymbol{q} = \{\boldsymbol{u}, p\}$ by an extremely small amplitude 3D disturbance, $\boldsymbol{q}' = \{\boldsymbol{u}', p'\}$. The linearised non-dimensional governing equations (LNSE)

describing the perturbation evolution obtained by using this decomposition in equation 2 is given by

$$\frac{\partial \boldsymbol{u}'}{\partial t} = -(\boldsymbol{U}\cdot\boldsymbol{\nabla})\boldsymbol{u}' + (\boldsymbol{u}'\cdot\boldsymbol{\nabla})\boldsymbol{U} - \boldsymbol{\nabla}p' + \frac{1}{Re}\nabla^2\boldsymbol{u}'. \quad (4)$$

These equations can then be framed into an eigenvalue problem using a Fourier decomposition for the perturbations to predict the fastest-growing mode as a function of *Re* and spanwise wavenumber k. The stability threshold is determined by the minimum Reynolds number producing a non-negative growth rate for any k [1].

To study the receptivity and sensitivity of the flow to initial condition, momentum forcing or base flow variation, the adjoint LNSE and the global mode of the adjoint operator (the adjoint mode) are obtained. The adjoint LNSE are

$$\frac{\partial \boldsymbol{u}^*}{\partial t} = (\boldsymbol{U}\cdot\boldsymbol{\nabla})\boldsymbol{u}^* - (\boldsymbol{u}^*\cdot\boldsymbol{\nabla})\boldsymbol{U} + \boldsymbol{\nabla}p^* - \frac{1}{Re}\nabla^2\boldsymbol{u}^*. \quad (5)$$

The amplitude of a global mode and its dependence on initial condition ($\hat{\boldsymbol{u}}_0$) and momentum forcing ($\hat{\boldsymbol{f}}$) can be expressed as

$$A_l = \int \hat{\boldsymbol{u}}_l^* \cdot [\hat{\boldsymbol{u}}_0 + \hat{\boldsymbol{f}}]\, \mathrm{d}S \Big/ \int \hat{\boldsymbol{u}}_l^* \cdot \hat{\boldsymbol{u}}_l\, \mathrm{d}S. \quad (6)$$

The structural sensitivity (S_l) of an eigenvalue (σ_l) to any localised perturbation of the LNSE operator is given by

$$S_l(x,y) = |\hat{\boldsymbol{u}}_l||\hat{\boldsymbol{u}}_l^*| \Big/ \int \hat{\boldsymbol{u}}_l^* \cdot \hat{\boldsymbol{u}}_l\, \mathrm{d}S. \quad (7)$$

Further details can be found in [4].

Numerical Method

An in-house solver is used, based on a nodal spectral element method for spatial discretisation and a third order backward multistep method for time integration [7]. Forward and adjoint eigenvalue problems are solved via an implicitely restated Arnoldi iteration method [12]. The solver has been validated for numerous flow simulations [3, 15] and stability analysis problems [14, 13].

After a mesh resolution study, 594 element mesh with polynomial order 15 for the base flow and eigenvalue computations are adopted for $\beta = 0.25$. For other β and γ cases, meshes were constructed such that the size of the smallest element along the boundaries and largest elements remained the same as the one tested for grid resolution. The order of polynomial for the base flow and eigenvalue computation for all the cases were also kept similar to the tested mesh. Table 1 shows solution convergence with increasing element polynomial order for a test case having $\beta = 0.25$, $\gamma = 2$ and $Re = 400$. For calculating the growth rate for a spanwise wavenumber of $k = 1$, base flow solutions using polynomial order 15 was used. Note that for all the results, $\gamma = 2$, unless specified otherwise.

n_p	Nu	f	σ
8	2.428654	0.02801743	0.067914286
10	2.430494	0.02799898	0.067915247
12	2.431883	0.02801755	0.067916422
15	2.433943	0.02801789	0.067917737
20			0.067917748

Table 1. Mesh resolution for different order of polynomial (n_p) for $\beta = 0.25$, $\gamma = 2$ and $Re = 400$. $k = 1$ for growth rate of the leading eigenmode.

Results and Discussions

Two-Dimensional Flow Regimes

At low *Re*, a single recirculation region is formed in front of the wedge (regime-1). With further increase in *Re*, another recirculation region is formed further downstream (regime-2) on the wedge taper. With increasing *Re* both these recirculation regions increase in size and merge to form a bigger recirculation region before the wedge (regime-3). In regime-4, flow separation occurs at the wedge tip, forming a secondary recirculation region immediately after the wedge tip and the flow becomes unsteady, with the secondary vortex oscillating in length. Further increase in *Re* (regime-5) causes the vortex to deattach itself from the tip and a self sustained vortex shedding is observed. For higher blockage from $\beta = 0.5$, an additional regime (regime-2a) with a steady secondary recirculation region after the wedge tip is observed. The influence of *Re* for the onset of each of these regimes as a function of blockage is shown in figure 3.

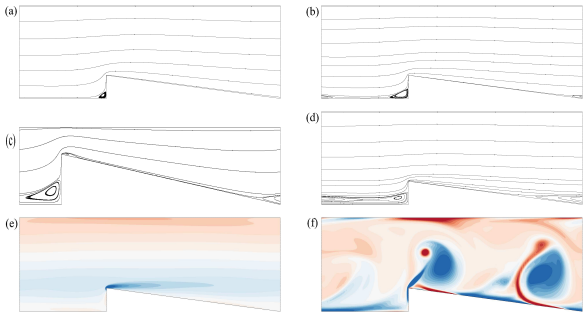

Figure 2. Two-dimensional flow regimes over repeated wedge shaped surface protrusions ($\beta = 0.25$, $\gamma = 2$) (a) Regime-1, $Re = 100$, (b) Regime-2, $Re = 175$, (c) Regime-2a for $\beta = 0.65$, $Re = 75$, (d) Regime-3, $Re = 200$, (e) Regime-4, $Re = 450$ and (f) Regime-5, $Re = 500$. Streamlines (a-d) and z-vorticity (c & d).

Heat Transfer Enhancement

To evaluate the effectiveness of these wedges for improving heat transfer from the heated walls to the fluid at the expense of the pumping power required to drive the fluid through the duct, enhancement ratio (ER) is calculated.. $ER > 1$ indicates enhancement with the use of the wedges and vice-versa. Figure 4 plots ER against *Re* covering the steady and unsteady regimes for a range of β and γ. In the steady regime, $ER < 1$ for all cases, and decreases with *Re*, indicating that the pressure drop is much higher than the corresponding increase in the heat transfer rate. With increasing *Re*, ER exceeds unity at different *Re* for each case. This jump starts with the onset of vortex shedding causing convective heat transfer to dominate over conductive heat trans-

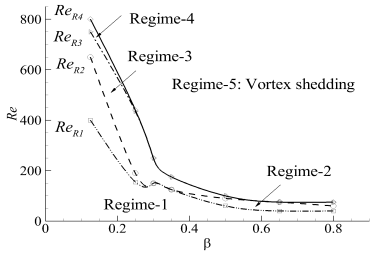

Figure 3. Regime map as function of *Re* and β. Re_i represents the *Re* for the onset of the next regime

fer. The vortices sweeping over the bottom walls and interacting with the vortices formed on the top wall results in better mixing between the cold and the hot fluid near the top and bottom walls, resulting in an increase in the bulk temperature of the fluid and temperature gradient at the walls. Figure 5 shows the temperature field for a steady case and an instantaneous snapshot with vortex shedding.

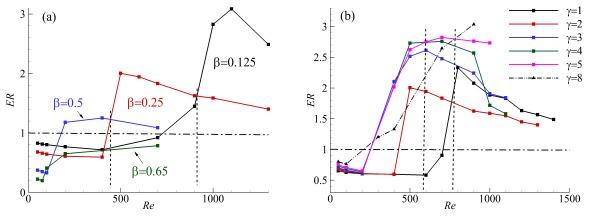

Figure 4. ER as a function of Re for different (a) blockage (β) and (b) pitch (γ).

In the range of β and γ investigated, the highest blockage, $\beta = 0.65$, is not effective to promote heat transfer effciency. From figure 4(a), it can be seen that with increasing Re the lower blockage becomes more effective as means to increase the efficiency. The dashed lines are used as indicators to show the approximate Re after which a lower β becomes more effective. In figure 4(b), the first dashed line from the right shows the approximate Re, up to which the optimal γ lies roughly between 4–5, above this range upto the next dashed line, the optimal γ shifts to a larger value around 5–8. Above this approximate threshold Re, lowering the distance between the wedges also has a favourable effect on the effciency as does increasing the distance.

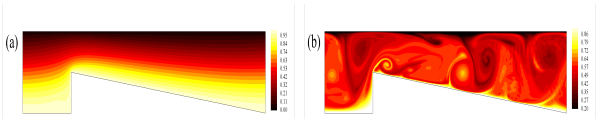

Figure 5. Temperature field for $\beta = 0.5$ (a) $Re = 100$ (steady) (b) $Re = 400$ (unsteady).

Linear Stability

The primary instability for the steady two-dimensional flow over repeated wedges in a duct occurs through a three-dimensional steady mode for all blockage and pitch investigated here. The values of the critical Reynolds number (Re_{cr}) and critical wavenumber (k_{cr}) for the onset of instability are shown in table 2.

Figure 6 (a & b) shows iso-contours of streamwise vorticity of the leading eigenmodes for $\beta = 0.25$ and $\beta = 0.5$. For both cases the leading mode is concentrated near the wedge, consisting of a pair of counter-rotating streamwise vortices before the wedge and a pair from the front of the wedge extending over it. For $\beta >= 0.5$, an additional pair of streamwise vortices emerge near the top wall above the wedge. Iso-contours of the streamwise velocity shows fast and slow moving streaks extending through the flow domain and spanwise velocity component of the eigenmodes concentrated near the wedge, inside the primary re-circulation region extending over the wedge with no significant spanwise velocity component observed inside the recirculation region formed after the wedge tip (figure 6 (c)).

These eigenmodes resemble the leading eigenmodes seen in forward facing step (FFS) [11] and backward facing step (BFS) for blockage of 0.25 [1, 10] and also matches with experimental observation in [17]. Lanzerstorfer and Kuhlmann [11] from their analysis for a FFS concluded that a lift-up mechanism along with flow decelaration was the cause of the instability. For flow around a 180^o bend [14] an elliptic instability mechanism in a re-circulation region behind the corner was responsible for the instability. The velocity components of the perturbation indicates a lift-up mechanism [9] responsible for the instability where a small transverse perturbation moves the fluid to a high velocity region leading to the formation of streaks, which decays downstream.

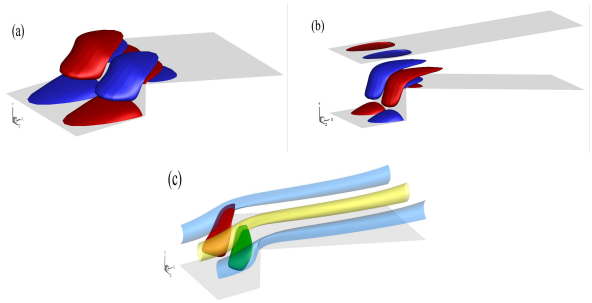

Figure 6. 3D iso-surface of streamwise vorticity for (a) $\beta = 0.25$, $Re = 400$, (b) $\beta = 0.5$, $Re = 100$ (c) Iso-surface of streamwise (x) and spanwise velocity (z) of the eigenmodes for $\beta = 0.5$, $Re = 100$, represented as translucent and opaque surfaces respectively.

Blockage	Re_{cr}	k_{cr}	Pitch	Re_{cr}	k_{cr}
0.125	162.22	1.82295	1	79.4	1.74095
0.25	86.85	1.72921	2	86.85	1.72921
0.35	71	1.75209	4	100.49	1.74665
0.5	58.59	1.95534	8	127.42	1.76608
0.65	55.15	2.21249			
0.8	57.98	2.65795			

Table 2. Critical Reynolds number and wavenumber for different blockage and pitch.

For all blockage and pitch values investigated, onset of 2D unsteadiness was not associated with a linear instability mode; instead, this onset may be explained by a sensitivity analysis.

Receptivity and Sensitivity

An adjoint analysis is carried out to obtain regions in the flow which are receptive to inital condition/ momentum forcing. For $\beta = 0.5$ and $Re = 100$, this region of maximum adjoint velocity amplitude is in the core of the flow extending from above the wedge tip to about half way downstream for a two-dimensional perturbation as shown in figure 7(a) and is where any localised intial perturbation would lead to maximum amplification of the global mode. Any kind of momentum forcing will be more beneficial in terms of amplifying the global mode if placed in these regions. The feedback region, where there is maximum coupling between the receptive region and amplifier regions makes the largest impact on the leading eigenvalue and thus shows the core of the instability mechanism, responsible for a self-sustained instability in the two-dimensional steady flow. Figure 7(b) shows the sensitivity of the two-dimensional steady flow to local base flow modifications under equation 7. The core of the instability which gives rise to a self-sustained 2D vortex shedding is located downstream of the wedge tip extending to the front of the next wedge.

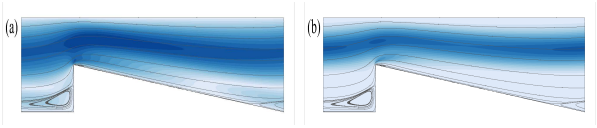

Figure 7. (a) Receptivity to initial condition/momentum forcing, (b) sensitivity to base flow modification for $\beta = 0.5$, $Re = 100$.

Three-dimensional simulation

Three-dimensional direct numerical simulation was performed with spanwise periodicity matching the wavelength of the dominant instability mode. 16 Fourier modes were found to be sufficient to resolve the flow. Growth rate and structure of the 3D disturbance matched the linear prediction. Remnants of the eigenmode structure persists through non-linear saturation of the mode (figure 8 (a); $Re = 100$, $\beta = 0.5$). The corresponding temperature field (figure 8 (b)) demonstrates streamwise vortices and plumes enhancing vertical mixing and heat transfer. For $Re = 100$ and $\beta = 0.5$, the time-averaged Nusselt number and friction factor for 3D simulations is approximately 1.8 and 1.34 times the corresponding 2D case.

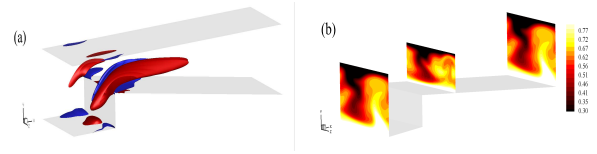

Figure 8. (a) Iso-contours of streamwise vorticity (b) Temperature field at $x = 0.0$, 4.0 and 10.0 units for $\beta = 0.5$, $Re = 100$.

Conclusions

The enhancement in the heat transfer efficiency with the use of repeated wedge shaped surface protrusions and an approximate range of parameters where maximum effectiveness can be obtained are elucidated. Breakdown of the two-dimensional solutions to infinitesimal three-dimensional perturbations are found to occur through a steady mode. Onset of three dimensionality happens due to a lift-up mechanism which is sustained by the primary recirculation region. It was shown that the 2D steady to unsteady transition occurs due to the sensitivity of the flow to incoming perturbation created by the wedge upstream. Favourable locations to place any flow control mechanism to affect the flow's stability is in the core of the flow domain, downstream from the wedge tip. Furthermore, increasing three-dimensionality in the flow is a favorable condition to increase the heat transfer enhancement ratio.

Acknowledgements

S.M. receives an Australian Government RTP and Monash International Tuition Scholarship. This research is supported by Australian Research Council Discovery Grant DP180102647, the National Computational Infrastructure, Pawsey Supercomputing Centre, and the Monash MonARCH machine.

References

[1] Barkley, D., Gomes, M. G. M. and Henderson, R. D., Three-dimensional instability in flow over a backward-facing step, *J. Fluid Mech.*,, **473**, 2002, 167–190.

[2] Bhagoria, J., Saini, J. and Solanki, S., Heat transfer coefficient and friction factor correlations for rectangular solar air heater duct having transverse wedge shaped rib roughness on the absorber plate, *Renew. Energy*, **25**, 2002, 341–369.

[3] Cassells, O. G. W., Hussam, W. K. and Sheard, G. J., Heat transfer enhancement using rectangular vortex promoters in confined quasi-two-dimensional magnetohydrodynamic flows, *Int. J. Heat Mass Transf.*, **93**, 2016, 186–199.

[4] Giannetti, F. and Luchini, P., Structural sensitivity of the first instability of the cylinder wake., *J. Fluid Mech.*, **581**, 2007, 167–197.

[5] Hamid, A. H. A., Hussam, W. K. and Sheard, G. J., Heat transfer augmentation of a quasi-two-dimensional MHD duct flow via electrically driven vortices, *Numer. Heat Tranf. A-Appl.*, **70**, 2016, 847–869.

[6] Huang, H. and Li, B., Heat transfer enhancement of MHD flow by conducting strips on the insulating wall, *J. Heat Transf.-Trans. ASME*, **133**, 2011, 021902.

[7] Karniadakis, G. and Sherwin, S., *Spectral/hp element methods for computational fluid dynamics*, Oxford University Press, 2013.

[8] Karwa. and Rajendra., Experimental studies of augmented heat transfer and friction in asymmetrically heated rectangular ducts with ribs on the heated wall in transverse, inclined, v-continuous and v-discrete pattern, *Int. Commun. Heat Mass*, **30**, 2003, 241–250.

[9] Landahl, M., Wave breakdown and turbulence, *SIAM J. Appl. Math.*, **28**, 1975, 735–756.

[10] Lanzerstorfer, D. and Kuhlmann, H. C., Global stability of the two-dimensional flow over a backward-facing step, *J. Fluid Mech.*, **693**, 2012, 1–27.

[11] Lanzerstorfer, D. and Kuhlmann, H. C., Three-dimensional instability of the flow over a forward-facing step, *J. Fluid Mech.*, **695**, 2012, 390–404.

[12] Lehoucq, R. B., Sorensen, D. C. and Yang, C., *ARPACK users' guide: solution of large-scale eigenvalue problems with implicitly restarted Arnoldi methods*, volume 6, Siam, 1998.

[13] Ng, Z., Vo, T. and Sheard, G., Stability of the wakes of cylinders with triangular cross-sections., *J. Fluid Mech.*, **844**, 2018, 721.

[14] Sapardi, A. M., Hussam, W. K., Pothérat, A. and Sheard, G. J., Linear stability of confined flow around a 180-degree sharp bend, *J. Fluid Mech.*,, **822**, 2017, 813–847.

[15] Sheard, G. J., Wake stability features behind a square cylinder: focus on small incidence angles, *J. Fluids Struct.*, **27**, 2011, 734–742.

[16] Smolentsev, S., Moreau, R., Bühler, L. and Mistrangelo, C., MHD thermofluid issues of liquid-metal blankets: phenomena and advances, *Fusion Eng. Des.*, **85**, 2010, 1196–1205.

[17] Stüer, H., Gyr, A. and Kinzelbach, W., Laminar separation on a forward facing step, *Eur. J. Mech. B-Fluids*, **18**, 1999, 675–692.